Perspectives of fast magic-angle spinning ^{87}Rb NMR of organic solids at high magnetic fields

Gang Wu, Victor V. Terskikh, Alan Wong

Perspectives of fast magic-angle spinning ^{87}Rb NMR of organic solids at high magnetic fields

Gang Wu[1] **Victor Terskikh**[1,2] **Alan Wong**[1]

Abstract

We report solid-state ^{87}Rb NMR spectra from two Rb-ionophore complexes obtained with fast magic-angle spinning (MAS) (up to 60 kHz) at 21.1 T. These Rb-ionophore complexes containing macrocycles such as benzo-15-crown-5 and cryptand [2.2.2] are typical of organic Rb salts that exhibit very large ^{87}Rb quadrupole coupling constants (close to 20 MHz). We have also obtained static ^{87}Rb NMR spectra for these two compounds and determined both ^{87}Rb quadrupole coupling and chemical shift tensors. The experimental ^{87}Rb NMR ten-sor parameters are compared with those obtained by quantum chemical computations. Our results demonstrate that the combination of fast MAS (60 kHz or higher) and a high magnetic field (21.1 T or higher) is sufficient to produce high-quality solid-state ^{87}Rb NMR spectra for organic Rb solids at the natural abundance level. We anticipate that, with additional ^{87}Rb isotope enrichment (up to 99%), the sensitivity of solid-state ^{87}Rb NMR will be 400 times higher than ^{39}K NMR, which makes the former an attractive surro-gate probe for studying K^+ ion binding in biological systems.

Although it is a rather routine exercise to record solid-state ^{87}Rb NMR spectra for simple inorganic Rb salts, far fewer examples are available in the literature for solid-state ^{87}Rb NMR studies of organic Rb salts.[1] In general, Rb^+ ions in the majority of inorganic salts experience rather symmetric environments resulting in relatively small ^{87}Rb quadrupole coupling (QC) constants, $C_Q(^{87}Rb)$. For example, one of the most commonly used test samples in solid-state ^{87}Rb NMR experiments is $RbNO_3$, where the three crystallographic distinct Rb sites all have $C_Q(^{87}Rb)$ values on the order of 2 MHz. In contrast, the $C_Q(^{87}Rb)$ values in many organic Rb salts often exceed 10 MHz.[1] As a result, it is not always possible to obtain high-quality magic-angle spinning (MAS) ^{87}Rb NMR spectra for these organic systems because the static second-order quadrupole line width associated with a large $C_Q(^{87}Rb)$ value is often considerably greater than any practical sample spinning frequency. In an early solid-state ^{87}Rb NMR study, Cheng et al.[2] examined the orientations of the ^{87}Rb QC and chemical shift (CS) tensors for a number of Rb compounds including two simple organic salts: Rb (acetate)·H_2O and Rb (formate)·H_2O. In these two Rb salts, the values of $C_Q(^{87}Rb)$ are relatively small, <7 MHz. Kim et al.[3] used solid-state ^{87}Rb NMR for stationary samples to probe the formation of alkalides and electrides, for which the values of $C_Q(^{87}Rb)$ were found to be as large as 17 MHz. Solid-state ^{87}Rb NMR was also used to study ion binding

in G-quadruplexes[4–6] and cation-π interactions.[7] Nonetheless, solid-state ^{87}Rb NMR has yet to find a wide use in studying organic and biological solids.

The primary motivation for the present work is to demonstrate the potential of solid-state ^{87}Rb NMR in studying organic metal complexes as well as to examine the possibility of using solid-state ^{87}Rb NMR as a surrogate probe for studying K^+ ion-binding sites in biologically relevant systems. As one of the low-γ quadrupolar nuclei, ^{39}K is notoriously difficult to study by NMR. Table 1 shows some basic NMR properties of ^{39}K, together with those for two magnetically active Rb isotopes, ^{85}Rb and ^{87}Rb. First, the low ^{39}K NMR frequency not only makes the overall NMR sensitivity very low but also causes severe second-order quadrupole broadening, because the second-order quadrupole broadening is inversely proportional to the NMR frequency of the nucleus under observation. Second, the ^{39}K chemical-shift range (<150 ppm) usually is smaller than the second-order quadrupole broadening, causing the poor site resolution in solid-state ^{39}K NMR spectra. For these reasons, solid-state ^{39}K NMR experiments are often time-consuming and produce very broad spectra at low and moderate magnetic fields (e.g., 11.75 T). In recent years, as a result of the increasing availability of high magnetic fields, considerable progress has been made in solid-state ^{39}K NMR studies of organic systems.[8–15] However, the small chemical-shift range of ^{39}K remains to be an obstacle to further biological applications. It is well known that, within the alkali metal group, Rb^+ is more similar to K^+ than is Na^+. For example, Rb^+ has an ionic radius of 1.48 Å, comparable with that of K^+, 1.33 Å, whereas the ionic radius of Na^+ is much smaller, 0.95 Å.[16] In crystals, the average observed coordination numbers for Na^+, K^+, and Rb^+ are 6.7, 9.0, and 9.8, respectively.[16] In aqueous solution, the first hydration shell of Na^+ typically contains six water molecules.[17] For K^+, the corresponding number is typically between 7 and 8, which is once again closer to that seen for Rb^+, 8.[18] Another property of metal ions that plays a key role in metal ion binding processes in biological systems is the so-called free energy of hydration (ΔG_{hyd}). The ΔG_{hyd} values for Na^+, K^+, and Rb^+ ions are −98.2, −80.6, and −75.5 kcal/mol, respectively, so in this aspect, K^+ is better modeled by Rb^+ than by Na^+.[19] For these reasons, Rb^+ is known to be a better mimic of K^+ than is Na^+ in many chemical and biological processes.

As also seen from Table 1, the NMR receptivity of ^{87}Rb is nearly 100 times higher than that of ^{39}K. With further ^{87}Rb isotope enrichment (up to 99%), ^{87}Rb NMR would be about 400 times more sensitive than ^{39}K (natural abundance 93.26%) NMR.[1] In addition, the relatively large ^{87}Rb chemical-shift range (ca. 400 ppm) makes ^{87}Rb NMR signals potentially more sensitive to the chemical environment around the Rb^+ ion. Indeed, Rb^+ has been used as a K^+ congener in solution NMR and MRI studies.[20–25] In the context of solid-state NMR, although the line-width factor in the central-transition (CT) ^{87}Rb NMR is four times of that for ^{39}K,[1] the combination of a higher sensitivity and greater resolving power still makes ^{87}Rb NMR an attractive surrogate probe for studying K^+ binding environment. It should be noted that ^{85}Rb is also an NMR-active isotope, $I = 5/2$. However, the sensitivity of ^{85}Rb NMR is much lower than that of ^{87}Rb NMR because of the fact that the quadrupole moment of ^{85}Rb is two times larger than that of ^{87}Rb and the magnetogyric ratio of ^{85}Rb is nearly four times smaller. In addition, because the receptivity of CT is inversely proportional to $I(I + 1)$,[1] the sensitivity of detecting the CT for ^{85}Rb is further reduced by a factor of $7/3 \approx 2.3$ as

TABLE 1 Nuclear spin properties, line-width factors, NMR receptivity, and reference samples for stable and magnetically active K and Rb isotopes

	^{39}K	^{85}Rb	^{87}Rb
Nuclear spin, I	3/2	5/2	3/2
Natural abundance, %	93.26	72.17	27.83
$\gamma/10^7$ rad T^{-1} s^{-1}	1.2500608	2.5927050	8.786400
Frequency ratio, Ξ/%	4.666373	9.654943	32.720454
Q/mb (1 mb = 10^{-31} m^2)	58.5	276	133.5
$1 - \gamma_\infty$	22.8	53.8	53.8
CT line width factor,[a] l_{CT}	107	1531	440
Receptivity ratio for CT,[a] D_{CT}^C	0.558	3.86	58.0
Primary reference sample, $\delta = 0$ ppm	KCl in D_2O, 0.1 mol/dm^3	RbCl in D_2O, 0.1 mol/dm^3	
Secondary reference sample for solid-state NMR	KBr(s) at 56.2 ppm	RbCl(s) at 128.1 ppm	

[a]The unit of l_{CT} is 10^{-3} fm^4 rad^{-1} T s. See Wu and Zhu[1] for discussion of l_{CT} and D_{CT}^C.

compared with that for the CT of a spin-3/2 nucleus. After considering all the factors, the receptivity of ^{85}Rb CT is more than 15 times lower than that for ^{87}Rb CT, as seen in Table 1.

To reduce the second-order quadrupole broadening in CT-based solid-state NMR, it is critical to use ultrahigh magnetic fields.[26–28] In this work, we combine a high magnetic field of 21.1 T with fast MAS (60 kHz) to record solid-state ^{87}Rb NMR spectra from two prototypical Rb-ionophore complexes: $Rb(B15C5)_2Br{\cdot}H_2O$ and Rb(C222)$SCN{\cdot}H_2O$ (Scheme 1). These systems were chosen because they are known to have very large $C_Q(^{87}Rb)$ values (on the order of 15–20 MHz).[1] As a result, ^{87}Rb MAS NMR spectra have not yet been reported for this type of compounds in the literature.

2 EXPERIMENTAL SECTION

2.1 Synthesis

Benzo-15-crown-5 (B15C5) and cryptand [2.2.2] (C222) were purchased from Aldrich (Ontario, Canada). Following the general literature procedures,[3] crystalline Rb ionophore complexes were prepared by crystallization at room temperature from a salt/ligand mixture of a suitable molar ratio in methanol. The two compounds were found to be very stable. No spectral change was observed even after the samples were spun at 60 kHz for 24 h.

2.2 Solid-state ^{87}Rb NMR

Solid-state ^{87}Rb NMR experiments were performed on Bruker Avance-500 (11.75 T) and Avance-II 900 (21.1 T) spectrometers operating at 163.65 and 294.51 MHz, respectively. Static experiments at 11.75 T were performed with a Bruker 4-mm H/X MAS probe. Proton decoupling of 80 kHz was applied during data acquisition. MAS experiments at 21.1 T were carried out with Bruker 2.5- and 1.3-mm H/X MAS probes. All ^{87}Rb MAS spectra were recorded using a Hahn-echo sequence with the first pulse delay being set to one rotor rotation period. To reduce frictional heating during the fast MAS experiments, the sample was cooled to about the room temperature using a Bruker BCU05 cooling unit. Static ^{87}Rb experiments at 21.1 T were acquired with a Bruker 2.5-mm H/X MAS probe. Proton decoupling of 120 kHz was applied during data acquisition. All ^{87}Rb chemical shifts were referenced to the ^{87}Rb NMR signal from 1 M $RbNO_3$(aq). Solid-state ^{87}Rb NMR spectra were analyzed using DMFit.[29]

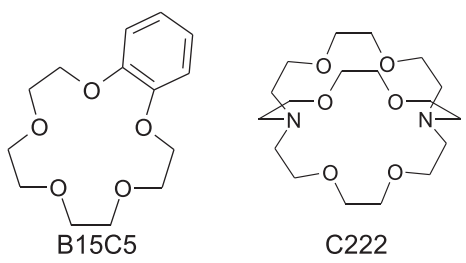

SCHEME 1 Molecular structures of the two macrocyclic ionophore ligands studied in this work

2.3 Quantum chemical computation

Plane-wave pseudopotential DFT calculations of the NMR magnetic shielding and QC parameters were performed using Materials Studio CASTEP software version 4.4 (Accelrys)[30] installed on an HP xw4400 workstation with a single Intel Dual-Core 2.67 GHz processor and 8 GB DDR RAM. The Perdew, Burke, and Ernzerhof functionals were used in all calculations in the generalized gradient approximation for the exchange–correlation energy. On-the-fly pseudopotentials were used as supplied with NMR CASTEP with a plane-wave basis set cut-off energy of 300 eV and Monkhorst–Pack *k*-space grid sizes of 2 × 2 × 2 (four *k*-points used). CASTEP calculations were based on the reported crystal structures for $Rb(C222)SCN{\cdot}H_2O$ (CCDC-1247406)[31] and $Rb(B15C5)_2NO_3{\cdot}H_2O$ (CCDC-1158666).[32] Because the original crystal structures did not include hydrogen atoms, we have calculated their positions using Materials Studio. Because of the very large unit cell sizes of both crystal structures, CASTEP calculations were performed with single molecules in a pseudotriclinic space group P1 unit cell of sufficient volume, for example, 12 Å × 12 Å × 12 Å, to avoid intermolecular interactions. To preserve the charge balance for chemical shielding computations, the counter anions were kept in the unit cell. The crystal structures from the literature were directly employed in the CASTEP computations without geometry optimization. In fact, we found that geometry optimization produced significantly poorer agreement with the experimental NMR results. This may be because both the B15C5 and C222 ligands are quite flexible. To convert computed absolute ^{87}Rb magnetic shielding constants (σ) to the ^{87}Rb chemical shifts (δ), we used $\delta = \sigma_{ref} - \sigma$ where $\sigma_{ref}(^{87}Rb) = 3213.4$ ppm (*vide infra*). This $\sigma_{ref}(^{87}Rb)$ value is nearly the same as that reported by de Dios et al., 3213 ppm, which was calculated for $[Rb(H_2O)_6]^+$ at the Hartree–Fock level.[33] We should note that, because the version of CASTEP software used an older value of the ^{87}Rb nuclear quadrupole moment, $Q(^{87}Rb) = 13.2 \times 10^{-30}$ m^2, we scaled up the CASTEP

computed $C_Q(^{87}Rb)$ values by using the latest $Q(^{87}Rb)$ value, 13.35×10^{-30} m^2.[34]

3 RESULTS AND DISCUSSION

Figure 1 shows ^{87}Rb MAS NMR spectra of Rb(B15C5)$_2$Br·H$_2$O at 21.1 T. When the sample spinning frequency is 35 kHz, significant intensities are observed on the spinning sidebands, so that the central band partially overlaps with the sidebands. When the sample spinning is increased to 60 kHz, the intensities of the sidebands become almost negligible, resulting in a well-defined central band of characteristic line shape because of the second-order quadrupole interaction. Spectral fitting produces the following ^{87}Rb NMR parameters for Rb (B15C5)$_2$Br·H$_2$O: $\delta_{iso} = -5 \pm 2$ ppm, $|C_Q| = 13.2 \pm 0.5$ MHz, and $\eta_Q = 0.78 \pm 0.05$. Kim et al.[3] obtained static ^{87}Rb NMR spectra for two related compounds, Rb(15C5)$_2$Cl and [Rb(15C5)$_2$]Rb$^-$, but observed much smaller $C_Q(^{87}Rb)$ values, approximately 5–7 MHz. In addition, they reported that the $C_Q(^{87}Rb)$ values in the Rb(18C6)X series (X = Cl$^-$, Br$^-$, I$^-$, Na$^-$, Rb$^-$, e$^-$) are also on the order of 7–11 MHz. Thus, the relatively large $C_Q(^{87}Rb)$ value observed in Rb(B15C5)$_2$Br·H$_2$O suggests a much distorted geometry around the Rb$^+$ ion (*vide infra*).

Figure 2 shows the ^{87}Rb MAS NMR spectra for Rb(C222)SCN·H$_2$O. Again, the presence of strong spinning sidebands in the spectrum obtained with 35 kHz sample spinning complicates the spectral analysis. At 60 kHz, the sideband intensities are greatly reduced. From the ^{87}Rb MAS spectra of Rb(C222)SCN·H$_2$O, we obtained the following ^{87}Rb NMR parameters: $\delta_{iso} = 78 \pm 2$ ppm, $|C_Q| = 18.9 \pm 0.5$ MHz, and $\eta_Q = 0.08 \pm 0.05$. Kim et al.[3] examined static ^{87}Rb NMR spectra from several similar systems Rb(C222)X (X = Cl$^-$, Br$^-$, I$^-$, SCN$^-$) and found the $C_Q(^{87}Rb)$ values in the range between 15.1 and 16.6 MHz. The $C_Q(^{87}Rb)$ value seen in Rb(C222)SCN·H$_2$O in our study appears to the largest so far reported for Rb organic systems. We should also point out that, in both cases shown in Figures 1 and 2, the ^{87}Rb MAS spectra obtained at 35-kHz sample spinning appear to have better signal-to-noise ratios than those at recorded 60 kHz, even though less numbers of transients were accumulated. This is simply because different sizes of MAS rotors were used in these two experiments. We used 2.5- and 1.3-mm rotors for the 35- and 60-kHz MAS experiments, respectively. In general, the

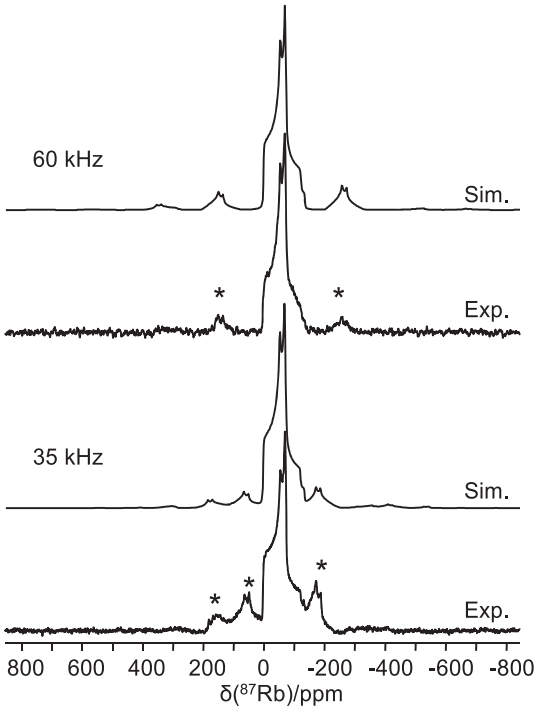

FIGURE 1 Experimental and simulated ^{87}Rb MAS NMR spectra of Rb(B15C5)$_2$Br·H$_2$O recorded at two sample spinning frequencies at 21.1 T. Spectral features due to spinning sidebands are marked by * in the experimental spectra. Other acquisition parameters are at 35 kHz, 10,000 transients, 0.5-s recycle delay and at 60 kHz, 20,000 transients, 0.5-s recycle delay

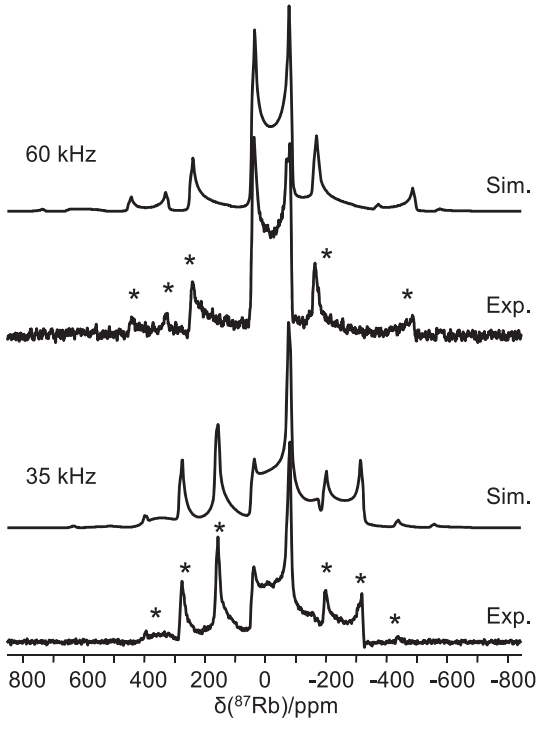

FIGURE 2 Experimental and simulated ^{87}Rb MAS NMR spectra of Rb(C222)SCN·H$_2$O recorded at two sample spinning frequencies at 21.1 T. Spectral features due to spinning sidebands are marked by * in the experimental spectra. Other acquisition parameters are at 35 kHz, 10,000 transients, 0.5-s recycle delay and at 60 kHz, 20,000 transients, 0.5-s recycle delay

amount of the solid compound packed into a 1.3-mm rotor is only 20% of that in a 2.5-mm rotor.

To accurately determine the ^{87}Rb CS tensors in the two complexes, we also obtained solid-state ^{87}Rb NMR spectra for static samples. As shown in Figure 3, the line shapes for nonspinning samples span about 500 ppm (approximately 150 kHz at 21.1 T). Spectral analysis allowed us to determine the ^{87}Rb CS tensor in each compound and their relative orientation with respect to that of the QC tensor. The Euler angles (ϕ, χ, ψ) used in the DMFit spectral simulations for Rb(B15C5)$_2$Br·H$_2$O and Rb(C222)SCN·H$_2$O are (0°, 85°, 0°) and (0°, 40°, 90°), respectively. These Euler angles are related to the more conventional set of Euler angles (α, β, γ)[35] in the following fashion: $\alpha = 90° - \psi$; $\beta = -\chi$; $\gamma = -\phi$. The other ^{87}Rb NMR tensor parameters obtained from this spectral analysis are summarized in Table 2. For both samples, the ^{87}Rb CS anisotropies are relatively small, but their contributions to the powder line shape become detectable at 21.1 T. The ^{87}Rb CS tensor parameters found for Rb(B15C5)$_2$Br·H$_2$O and Rb(C222)SCN·H$_2$O are comparable with those reported for simple Rb organic salts, Rb (acetate)·H$_2$O, and Rb (formate)·H$_2$O.[2] For example, we found that the span ($\Omega = \delta_{11} - \delta_{33}$) of the ^{87}Rb CS tensor for Rb(B15C5)$_2$Br·H$_2$O is 67 ppm, which would make a contribution of about 20 kHz at 21.1 T, which accounts for approximately 13% of the total line width. In contrast, ^{87}Rb static NMR spectra for these two compounds were also recorded at 11.75 T (data given in the Supporting Information).[36] The quality of the low-field static ^{87}Rb NMR spectra is similar to that reported by Kim et al.[3] for related Rb compounds. At 11.75 T, the total widths for the static ^{87}Rb CT spectra are on the order of 250–300 kHz, so a span of the ^{87}Rb CS tensor of 67 ppm would contribute only 11 kHz (less than 4% of the total line width). For these reasons, information about the ^{87}Rb CS tensor in these ionophore compounds was not available from the low-field static spectra. Thus, performing solid-state ^{87}Rb NMR at very high magnetic fields allows detection of relatively small CS anisotropies in the presence of very large C_Q values.

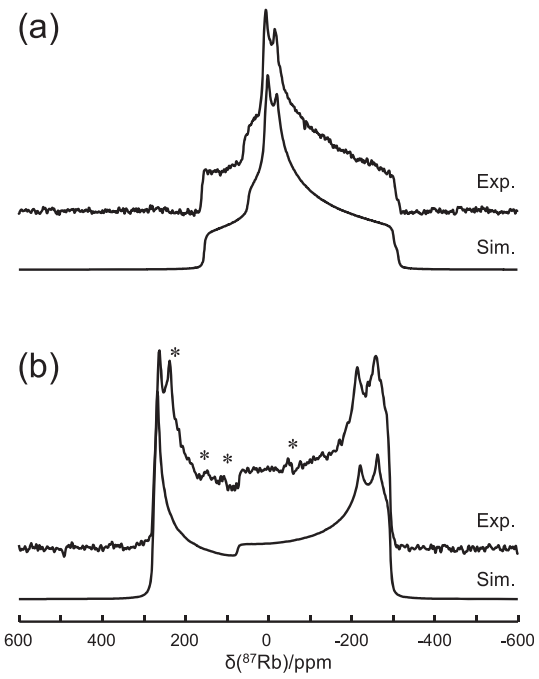

FIGURE 3 Experimental and simulated ^{87}Rb NMR spectra of static powder samples of (a) Rb(B15C5)$_2$Br·H$_2$O and (b) Rb(C222)SCN·H$_2$O at 21.1 T. In each case, 10,240 transients were accumulated with a recycle delay of 1 s. (b) Several sharp features marked by * were likely due to the presence of small microcrystallites

Figure 4 shows the correlation plot between computed ^{87}Rb magnetic shielding values and experimentally observed ^{87}Rb chemical shifts for the principal CS tensor components for Rb(B15C5)$_2$Br·H$_2$O and Rb(C222)SCN·H$_2$O. The y-intercept of the straight line shown in Figure 4 yields $\sigma_{ref} = 3213.4$ ppm, which was used in converting magnetic shielding results to the CS data reported in Table 2. Given the relatively large errors in the experimental values, the general agreement between the computed and observed data shown in Figure 4 is reasonable.

Now, we turn our attention to the ^{87}Rb QC and CS tensors observed for Rb(B15C5)$_2$Br·H$_2$O and Rb(C222)SCN·H$_2$O and their relationships with molecular structures. To facilitate discussion, we show in Figure 5 the orientations of the ^{87}Rb NMR tensors in the molecular frame of reference. The central Rb^+ ion in Rb(B15C5)$_2$Br·H$_2$O is sandwiched between two B15C5 ligands, coordinating to a total of 10 ether-oxygen atoms in a distorted pentagonal antiprism geometry. The Rb–O distances are in a range from 2.895 to 3.073 Å, with an average value of 2.981 Å.[32] The benzo groups of the two B15C5 ligands appear on the same side of the molecules. For Rb(C222)SCN·H$_2$O, the Rb^+ ion is inside the cage of C222, coordinating to six ether-oxygen atoms and two nitrogen atoms. The Rb–O distances are in the range between 2.879 and 2.898 Å with an averaged value of 2.888 Å, and the Rb–N distance is 3.011 Å.[31] The short Rb–O distances in Rb(C222)SCN·H$_2$O are clearly responsible for the observed ^{87}Rb isotropic CS of 78 ppm, which is considerably more deshielded than that found in Rb(B15C5)$_2$Br·H$_2$O. This trend is consistent with previous observations made in solid-state ^{23}Na and ^{133}Cs NMR studies of similar Na^+- and Cs^+-ionophore compounds.[37,38]

The absolute value of $C_Q(^{87}Rb)$ in Rb(C222)SCN·H$_2$O is significantly larger than that in Rb(B15C5)$_2$Br·H$_2$O, which reflects the fact that the

TABLE 2 Experimental[a] and CASTEP calculated ^{87}Rb CS and QC tensor parameters in Rb(B15C5)$_2$Br·H$_2$O and Rb(C222)SCN·H$_2$O

Compound		δ_{iso}/ppm	δ_{11}/ppm	δ_{22}/ppm	δ_{33}/ppm	C_Q/MHz[b]	η_Q
Rb(B15C5)$_2$Br·H$_2$O	Exptl	−5	24	4	−43	13.2	0.78
	CASTEP	−4	32	5	−50	10.78	0.78
Rb(C222)SCN·H$_2$O	Exptl	78	95	86	53	−18.9	0.08
	CASTEP	74	86	70	65	−17.76	0.11

[a]The uncertainties in the experimental data are δ_{iso}, ±2 ppm; δ_{ii}, ±10 ppm; C_Q, ±0.1 MHz; η_Q, ±0.05.
[b]The signs in the experimental C_Q values were assumed on the basis of CASTEP computations.

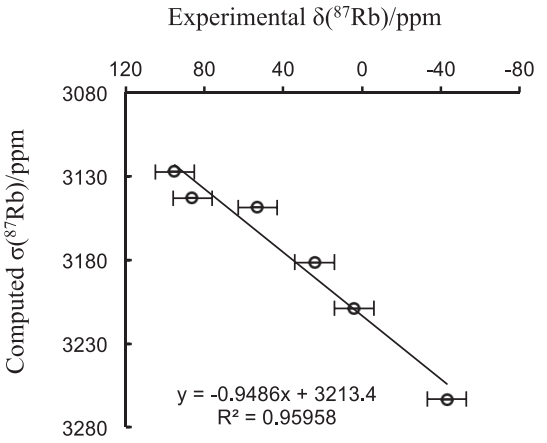

FIGURE 4 Plot of CASTEP computed absolute ^{87}Rb magnetic shielding (σ) values against experimental ^{87}Rb chemical shifts (δ) for Rb(B15C5)$_2$Br·H$_2$O and Rb(C222)SCN·H$_2$O. Note that, because the conversion between magnetic shielding (σ) and chemical shift (δ) follows $\delta = \sigma_{ref} - \sigma$, the *y*-intercept of the plot yields σ_{ref} = 3213.4 ppm

central Rb$^+$ ion inside the C222 cage experiences a highly asymmetrical environment (short Rb–O and long Rb–N bonds in the equatorial and axial directions, respectively). As seen from Figure 5, the [Rb(C222)]$^+$ structure has an approximate C_3 symmetry, and the largest ^{87}Rb QC tensor component is along the N–Rb–N direction. For this reason, the ^{87}Rb QC tensor in Rb(C222)SCN·H$_2$O is nearly axially symmetric (i.e., $\eta_Q \approx 0$). This situation is similar to the ^{23}Na QC tensor reported for [Na(C222)]$^+$ from a single-crystal ^{23}Na NMR study.[39] In contrast, the ^{87}Rb QC tensor in Rb(B15C5)$_2$Br·H$_2$O appears to be at another extreme (i.e., $\eta_Q \approx 1$). In this case, as seen in Figure 5, the largest ^{87}Rb QC tensor component points to the direction that is roughly normal to all the Rb–O bonds. It is also interesting to note that the C_Q(^{87}Rb) values in the two compounds exhibit opposite signs; see Table 2.

In general, the Townes–Dailey model can be used to provide an understanding about the QC tensors observed for covalent compounds.[40–42] For alkali metal ions, however, a much simpler point-charge model is often sufficient. According to the point charge model,[43] the largest electric-field-gradient (EFG) tensor component, V_{zz}, produced by the lattice can be calculated by

$$V_{zz} = \sum q_i \frac{3\cos^2\theta_i - 1}{r_i^3}, \quad (1)$$

where r_i and θ_i describe the distance and orientation of the *i*th effective point charge q_i with respect to the observing nuclear site. In the two Rb$^+$-ionophore complexes studied here, the ^{87}Rb QC tensors can be viewed as being entirely determined by the point partial charges at the oxygen and nitrogen atoms within the first-coordination sphere. Interestingly, in Rb(C222)SCN·H$_2$O, all six oxygen atoms appear nearly at the magic angle (54.7°) with respect to the N–Rb–N axis. This means that all the point charges from the oxygen atoms in Rb(C222)SCN·H$_2$O would contribute negligibly to the final ^{87}Rb QC tensor. This allows us to estimate the ^{87}Rb QC tensor simply from the contributions from the two axial nitrogen atoms. It can be readily shown that the V_{zz} produced at the Rb$^+$ ion from two nitrogen atoms in a linear N–Rb–N fragment is given by

$$V_{zz}\,(\text{a.u.}) = \frac{4\delta}{r^3}, \quad (2)$$

where δ is the point charge on the nitrogen atom and r is the distance between N and Rb$^+$. Note that all quantities in Equation 2 are expressed in the atomic units. Then the ^{87}Rb QC constant (in MHz) can be calculated as follows:

$$C_Q(\text{MHz}) = 2.349Q(1-\gamma_\infty)V_{zz} = 1.687\times10^3 V_{zz}(\text{a.u.}), \quad (3)$$

where the ^{87}Rb quadrupole moment Q is 13.35 fm^2,[34] the Sternheimer antishielding constant $(1 - \gamma_\infty)$ for ^{87}Rb is 53.8,[1] and the factor of 2.349 is from unit conversion. In Rb(C222)SCN·H$_2$O, the Rb–N distance is 3.011 Å. If we assume the point charge on the nitrogen atom to be

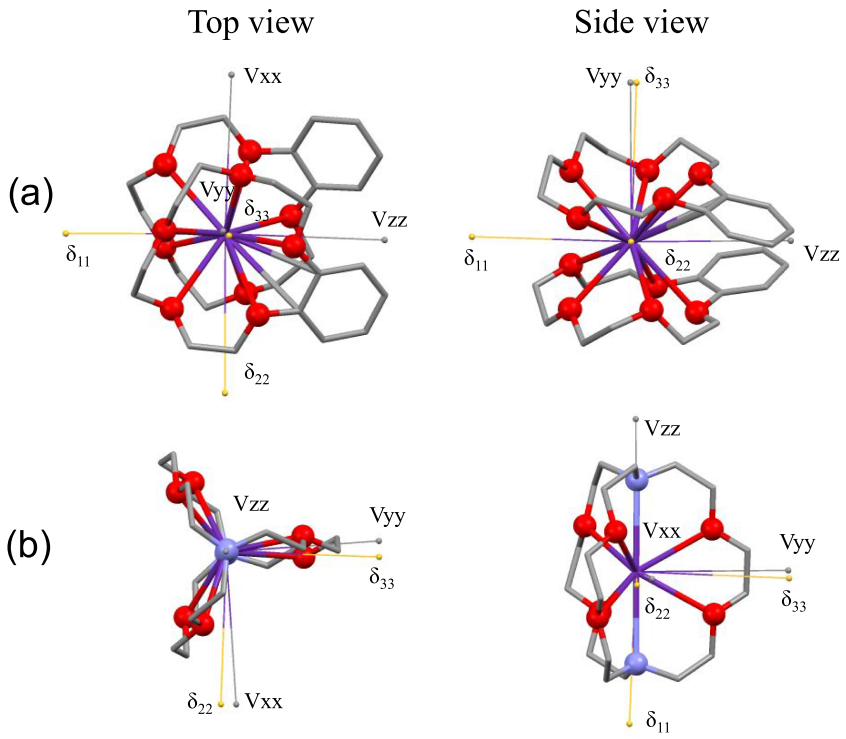

FIGURE 5 Top and side views of the ^{87}Rb QC and CS tensor orientations in the molecular frame of reference: (a) $Rb(B15C5)_2Br{\cdot}H_2O$ and (b) $Rb(C222)SCN{\cdot}H_2O$. Atoms in the first-coordination sphere around the Rb^+ ion (purple) are highlighted as balls (red, oxygen; blue, nitrogen). All hydrogen atoms are omitted for clarity

$\delta = -0.5$ a.u. (based on a Mulliken population analysis), one can estimate the value of $C_Q(^{87}Rb)$ to be −18.3 MHz, which is remarkably close to the experimental value, −18.9 MHz, and to the value computed by CASTEP. For $Rb(B15C5)_2Br{\cdot}H_2O$, because of the irregular arrangement of the 10 oxygen atoms, it is more difficult to visualize the ^{87}Rb QC tensor with a simplified model. Nonetheless, the point charge model predicts a $C_Q(^{87}Rb)$ value of 7.3 MHz if we assume $\delta = -0.7$ a.u. (based on a Mulliken population analysis) on each of the 10 oxygen atoms. This estimate, being about 30% smaller than the value computed by CASTEP, also illustrated the limitation of the point charge model.

Figure 5 also shows the orientations of the ^{87}Rb CS tensors in the molecular frame. In general, as noted previously,[2,44–47] ^{87}Rb CS and QC tensors may have different orientations. In the case of $Rb(B15C5)_2Br{\cdot}H_2O$, the two tensors have essentially the same orientation, as seen from Figure 5. The ^{87}Rb CS tensor component with the least shielding value, δ_{11}, is aligned with the largest QC tensor component, V_{zz}. The angle between δ_{33} of the ^{87}Rb CS tensor and V_{yy} of the QC tensor is only 5°. For $Rb(C222)SCN{\cdot}H_2O$, the ^{87}Rb QC tensor has its largest component along the approximate C_3 axis. Because the ^{87}Rb QC tensor is essentially axially symmetric ($\eta_Q = 0.08$), the angle between V_{yy} and δ_{33} is not well defined. We used a value of 40° for this angle to produce the simulated spectrum shown in Figure 3(b). Because the ^{87}Rb CS anisotropies are rather small in the two compounds studied here, we will not discuss them further.

It is also interesting to compare the ^{87}Rb quadrupole parameters observed for $Rb(C222)SCN{\cdot}H_2O$ with the corresponding ^{39}K quadrupole parameters for the K analog, K(C222)X. For the K^+ ions in the series of X = Na^-, K^-, e^-, Kim et al.[3] found that the $C_Q(^{39}K)$ values are in a narrow range between 2.65 and 2.72 MHz with $\eta_Q < 0.25$. For K(C222)I, Wong[36] reported that $C_Q(^{39}K) = 3.0$ MHz and $\eta_Q = 0.0$. Clearly, the approximate axial asymmetry holds for both ^{87}Rb and ^{39}K QC tensors. Furthermore, the $C_Q(^{87}Rb)/C_Q(^{39}K)$ ratios found in these structural analogs are also close to what is expected from the scaling factor of $(1 - \gamma_\infty)Q$, according to Equation 3. This means that the V_{zz} generated by the surrounding at the cation site is essentially the same in $Rb(C222)SCN{\cdot}H_2O$ and K(C222)X. Although this is just one data point, it nonetheless illustrates the possibility that Rb^+ can indeed serve as a surrogate probe for K^+.

To further establish the parallelism between ^{87}Rb and ^{39}K NMR parameters, we compiled a list of structurally related Rb and K inorganic salts for which both crystal and solid-state NMR data are available in the literature (see Tables S1–S3). In order to make direct comparison between ^{87}Rb and ^{39}K NMR quadrupole parameters, it is necessary to define the EFG generated by the crystal lattice (eq_{zz}^{latt}) in the following fashion:

$$eq_{zz} = eq_{zz}^{latt}(1-\gamma_{\infty}). \quad (4)$$

In general, the EFG experienced by the nucleus is larger than that produced by the surrounding crystal lattice because of the Steinheimer antishielding effect as mentioned earlier. In addition, it is well known that the lattice EFG contribution depends inversely on the unit cell volume.[48,49] As seen from Table S1, the unit-cell volumes for Rb salts are usually slightly larger than those for the corresponding K salts. As a result, K salts have slightly larger lattice EFG values than the Rb salts. To take this factor into consideration, we will scale the lattice EFG values for the K salts by the following expression:

$$eq_{zz}^{latt}(K)_{scaled} = eq_{zz}^{latt}(K)_{exp}\left(\frac{V_K}{V_{Rb}}\right), \quad (5)$$

where V_K and V_{Rb} are the unit-cell volumes for K and Rb inorganic salts, respectively. It is important to note that, because Rb^+ and K^+ have similar ionic radii, this scaling effect is only about 20%. Figure 6 shows the comparison between ^{87}Rb and ^{39}K NMR parameters for a series of structurally related Rb and K inorganic salts where Rb^+ and K^+ ions are coordinated to oxygen atoms. Indeed, both quadrupole parameters and chemical shifts are highly correlated between Rb and K salts. This provides strong evidence that ^{87}Rb NMR can indeed be used as a surrogate probe for studying the K ion binding environment in biologically relevant systems. In addition, as seen from Figure 6, the chemical shift range for ^{87}Rb is about 2.5 times larger than that for ^{39}K, suggesting that ^{87}Rb NMR is more sensitive to any subtle change in the ion-binding environment.

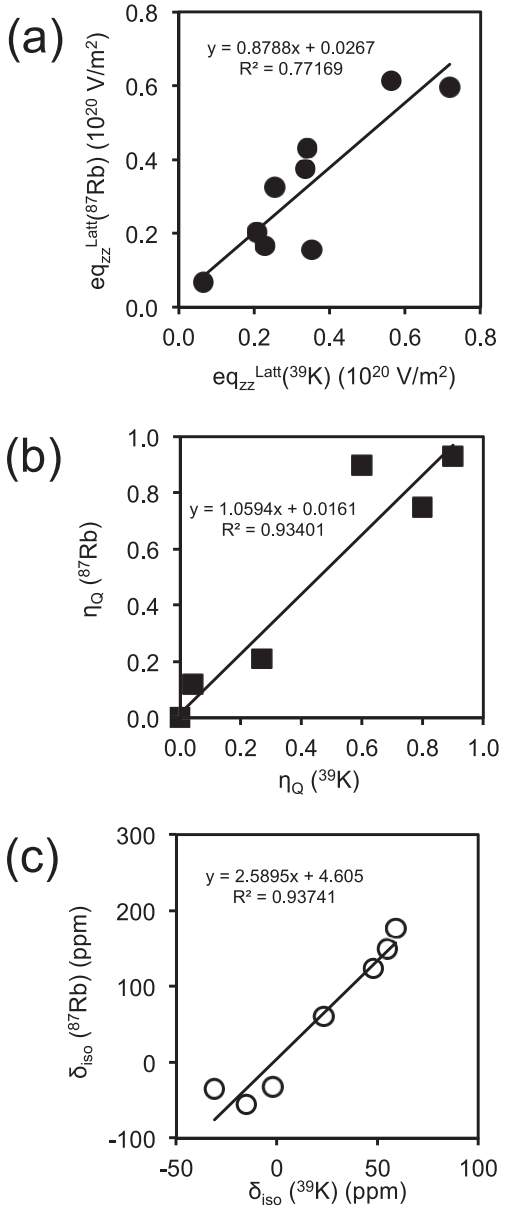

FIGURE 6 Comparison between ^{87}Rb and ^{39}K NMR properties for a series of structurally related Rb^+ and K^+ inorganic salts. All experimental values are listed in Tables S1–S3

Now, we discuss the issue of sensitivity. In the 60-kHz MAS experiments, only a very small amount of solid materials (1–2 mg) was used for each sample. However, high-quality ^{87}Rb MAS spectra were obtained after accumulation of 20,000 transients with a recycle time of 0.5 s (a total experimental time less than 3 h). If ^{87}Rb isotope enrichment of 99% is employed in sample preparation, one will be able to increase the sensitivity of ^{87}Rb NMR experiments by a factor of 4. That means that ^{87}Rb MAS spectra of the same quality as shown in Figures 1 and 2 can be obtained within 10 min for medium-size molecules (molecular masses of 500–700 Da). This sensitivity gain will make it possible to apply high-resolution methods such as MQMAS[50,51] and STMAS.[52] It is also possible to apply other techniques such as RIACT,[53] DFS,[54] FAM,[55] RAPT,[56] or HS[57] to further enhance the sensitivity of CT-based ^{87}Rb solid-state NMR, so that larger biomolecular systems can be tackled (e.g., to study K^+/Rb^+ ion binding to proteins).[58] In comparison, even the state-of-the-art solid-state ^{39}K NMR experiments so far reported in the literature typically employed a large amount of materials (ca. 50–100 mg) and long experimental times to compensate for the low intrinsic sensitivity.[13] Finally, one can also employ ^{1}H detection not only to enhance sensitivity but also to obtain information about heteronuclear ^{1}H–^{87}Rb correlation.[59–61]

4 CONCLUSIONS

We have obtained very fast MAS ^{87}Rb NMR spectra for two prototypical Rb-ionophore complexes at 21.1 T serving as models for biologically relevant systems. In these systems, the $C_Q(^{87}Rb)$ values were found to be on the order of 14–19 MHz, representing the largest values reported so far. Because of these large $C_Q(^{87}Rb)$ values, the total widths of the ^{87}Rb CT NMR signals for static powder samples usually exceed 100 kHz even at 21.1 T. As a result, MAS at least 60 kHz must be used to effectively reduce the intensities of spinning sidebands, making it easier for spectral analysis. We showed that, with only 1–2 mg of solid samples, high-quality ^{87}Rb MAS NMR spectra can be obtained reasonably quickly. The experimental time can be further shortened by approximately a factor of 16, if ^{87}Rb isotope enrichment up to 99% is used. We anticipate that the combination of ^{87}Rb isotope enrichment, fast (>60 kHz) MAS, and a high magnetic field (21.1 T or higher) will open new possibilities for making ^{87}Rb MAS NMR as an important tool in studying a wide range of chemical systems or as an effective surrogate probe for studying K^+ ion binding in biological systems.

ACKNOWLEDGEMENTS

This work was supported by the Natural Sciences and Engineering Research Council (NSERC) of Canada. Access to the 900-MHz NMR spectrometer was provided by the National Ultrahigh Field NMR Facility for Solids (Ottawa, Canada), a national research facility funded by a consor-tium of Canadian universities, National Research Council Canada and Bruker BioSpin and managed by the Univer-sity of Ottawa (http://nmr900.ca). We thank Dr. Ramsey Ida for assistance at the early stage of the work.

[1] G. Wu, J. Zhu, *Progr. Nucl. Magn. Reson. Spectrosc.* **2012**, *61*, 1.
[2] J. T. Cheng, J. C. Edwards, P. D. Ellis, *J. Phys. Chem.* **1990**, *94*, 553.
[3] J. Kim, J. L. Eglin, A. S. Ellaboudy, L. E. H. McMills, S. Z. Huang, J. L. Dye, *J. Phys. Chem.* **1996**, *100*, 2885.
[4] R. Ida, G. Wu, *Chem. Commun.* **2005**, 4294.
[5] A. Wong, R. Ida, G. Wu, *Biochem. Biophys. Res. Commun.* **2005**, *337*, 363.
[6] R. Ida, G. Wu, *J. Am. Chem. Soc.* **2008**, *130*, 3590.
[7] G. Wu, V. Terskikh, *J. Phys. Chem. A* **2008**, *112*, 10359.
[8] G. Wu, A. Wong, Z. H. Gan, J. T. Davis, *J. Am. Chem. Soc.* **2003**, *125*, 7182.
[9] A. Wong, R. D. Whitehead, Z. Gan, G. Wu, *J. Phys. Chem. A* **2004**, *108*, 10551.
[10] C. M. Widdifield, R. W. Schurko, *J. Phys. Chem. A* **2005**, *109*, 6865.
[11] I. L. Moudrakovski, J. A. Ripmeester, *J. Phys. Chem. B* **2007**, *111*, 491.
[12] P. K. Lee, R. P. Chapman, L. Zhang, J. Hu, L. J. Barbour, E. K. Elliott, G. W. Gokel, D. L. Bryce, *J. Phys. Chem. A* **2007**, *111*, 12859.
[13] G. Wu, Z. Gan, I. C. M. Kwan, J. C. Fettinger, J. T. Davis, *J. Am. Chem. Soc.* **2011**, *133*, 19570.
[14] K. Shimoda, A. Yamane, T. Ichikawa, Y. Kojima, *J. Phys. Chem. C* **2012**, *116*, 20666.
[15] G. J. Rees, S. P. Day, A. Lari, A. P. Howes, D. Iuga, M. B. Pitak, S. J. Coles, T. L. Threlfall, M. E. Light, M. E. Smith, D. Quigley, J. D. Wallis, J. V. Hanna, *CrystEngComm* **2013**, *15*, 8823.
[16] I. D. Brown, *Acta Cryst.* **1988**, *B44*, 545.
[17] Y. Marcus, *Chem. Rev.* **1988**, *88*, 1475.
[18] D. Z. Caralampio, J. M. Martinez, R. R. Pappalardo, E. Sanchez Marcos, *Phys. Chem. Chem. Phys.* **2017**, *19*, 28993.
[19] A. Wong, G. Wu, *J. Am. Chem. Soc.* **2003**, *125*, 13895.
[20] J. L. Allis, C. D. Snaith, A. M. L. Seymour, G. K. Radda, *FEBS Lett.* **1989**, *242*, 215.
[21] J. L. Allis, *Annu. Rep. NMR Spectrosc.* **1993**, *26*, 211.
[22] H. R. Cross, G. K. Radda, K. Clarke, *Magn. Reson. Med.* **1995**, *34*, 673.
[23] V. V. Kupriyanov, B. Xiong, J. Sun, O. Jilkina, G. Dai, R. Deslauriers, *Magn. Reson. Med.* **2001**, *46*, 963.
[24] V. V. Kupriyanov, M. L. H. Gruwel, *NMR Biomed.* **2005**, *18*, 111.
[25] V. E. Yushmanov, A. Kharlamov, T. S. Ibrahim, T. Zhao, F. E. Boada, S. C. Jones, *NMR Biomed.* **2011**, *24*, 778.
[26] Z. Gan, P. Gor'kov, T. A. Cross, A. Samoson, D. Massiot, *J. Am. Chem. Soc.* **2002**, *124*, 5634.
[27] Z. Gan, H. T. H. T. Kwak, M. Bird, T. A. Cross, P. Gor'kov, W. Brey, K. Shetty, *J. Magn. Reson.* **2008**, *191*, 135.
[28] Z. Gan, I. Hung, X. Wang, J. Paulino, G. Wu, I. M. Litvak, P. L. Gor'kov, W. W. Brey, P. Lendi, J. L. Schiano, M. D. Bird, I. R. Dixon, J. Toth, G. S. Boebinger, T. A. Cross, *J. Magn. Reson.* **2017**, *284*, 125.
[29] D. Massiot, F. Fayon, M. Capron, I. King, S. Le Calve, B. Alonso, J.-O. Durand, B. Bujoli, Z. Gan, G. Hoatson, *Magn. Reson. Chem.* **2002**, *40*, 70.
[30] S. J. Clark, M. D. Segall, C. J. Pickard, P. J. Hasnip, K. Refson, M. J. Probert, M. C. Payne, *Z. Kristallogr.* **2005**, *220*, 567.
[31] D. Moras, B. Metz, R. Weiss, *Acta Cryst.* **1973**, *B29*, 388.
[32] C. Momany, K. Clinger, M. L. Hackert, N. S. Poonia, *J. Incl. Phenom.* **1986**, *4*, 61.
[33] A. C. de Dios, A. Walling, I. Cameron, C. I. Ratcliffe, J. A. Ripmeester, *J. Phys. Chem. A* **2000**, *104*, 908.
[34] P. Pyykko, *Mol. Phys.* **2017**, *116*, 1328.
[35] G. Wu, *Prog. Nucl. Magn. Reson. Spectrosc.* **2008**, *52*, 118.
[36] A. Wong, M. Sc, *Thesis thesis, Queen's University*, Kingston, Ontario, Canada **2001**.

[37] A. Wong, G. Wu, *J. Phys. Chem. A* **2000**, *104*, 11844.
[38] A. Wong, S. Sham, S. N. Wang, G. Wu, *Can. J. Chem.* **2000**, *78*, 975.
[39] J. Kim, J. L. Dye, *J. Phys. Chem.* **1990**, *94*, 5399.
[40] C. H. Townes, B. P. Dailey, *J. Chem. Phys.* **1949**, *17*, 782.
[41] C. H. Townes, A. L. Schawlow, *Microwave Spectroscopy*, McGraw-Hill, Inc., New York **1955**.
[42] A. Rinald, G. Wu, *J. Phys. Chem. A* **2020**, *124*, 1176.
[43] E. A. C. Lucken, *Nuclear Quadrupole Coupling Constants*, Academic Press, New York, New York **1969**.
[44] W. P. Power, R. E. Wasylishen, S. Mooibroek, B. A. Pettitt, W. Danchura, *J. Phys. Chem.* **1990**, *94*, 591.
[45] T. Vosegaard, J. Skibsted, H. Bildsoe, H. J. Jakobsen, *J. Phys. Chem.* **1995**, *99*, 10731.
[46] T. Vosegaard, J. Skibsted, H. Bildsoee, H. J. Jakobsen, *J. Magn. Reson., Ser. A* **1996**, *122*, 111.
[47] T. Vosegaard, J. Skibsted, H. Bildsoe, H. J. Jakobsen, *Solid State Nucl. Magn. Reson.* **1999**, *14*, 203.
[48] R. Blinc, M. Mali, *Phys. Rev.* **1969**, *179*, 552.
[49] S. L. Segel, *J. Chem. Phys.* **1978**, *68*, 330.
[50] L. Frydman, J. S. Harwood, *J. Am. Chem. Soc.* **1995**, *117*, 5367.
[51] A. Medek, J. S. Harwood, L. Frydman, *J. Am. Chem. Soc.* **1995**, *117*, 12779.
[52] Z. Gan, *J. Am. Chem. Soc.* **2000**, *122*, 3242.
[53] G. Wu, D. Rovnyak, R. G. Griffin, *J. Am. Chem. Soc.* **1996**, *118*, 9326.
[54] A. P. Kentgens, R. Verhagen, *Chem. Phys. Lett.* **1999**, *300*, 435.
[55] P. K. Madhu, A. Goldbourt, L. Frydman, S. Vega, *Chem. Phys. Lett.* **1999**, *307*, 41.
[56] Z. Yao, H. T. Kwak, D. Sakellariou, L. Emsley, P. J. Grandinetti, *Chem. Phys. Lett.* **2000**, *327*, 85.
[57] R. Siegel, T. Nakashima, R. E. Wasylishen, *Chem. Phys. Lett.* **2004**, *388*, 441.
[58] M. J. Page, E. Di Cera, *Physiol. Rev.* **2006**, *86*, 1049.
[59] A. Venkatesh, M. P. Hanrahan, A. J. Rossini, *Solid State Nucl. Magn. Reson.* **2017**, *84*, 171.
[60] S. L. Carnahan, B. J. Lampkin, P. Naik, M. P. Hanrahan, I. I. Slowing, B. VanVeller, G. Wu, A. J. Rossini, *J. Am. Chem. Soc.* **2019**, *141*, 441.
[61] A. V. Wijesekara, A. Venkatesh, B. J. Lampkin, B. VanVeller, J. W. Lubach, K. Nagapudi, I. Hung, P. L. Gor'kov, Z. Gan, A. J. Rossini, *Chem. – Eur. J.* **2020**, *26*, 7881.